

pubs.acs.org/JACS Article

Photo-Uncaging by $C(sp^3)-C(sp^3)$ Bond Cleavage Restores β -Lapachone Activity

Esther G. Kaye, Bijan Mirabi, Ivonne R. Lopez-Miranda, Komadhie C. Dissanayake, Upasana Banerjee, Madelyn Austin, Mark Lautens, Arthur H. Winter, and Andrew A. Beharry*



Cite This: J. Am. Chem. Soc. 2023, 145, 12518-12531



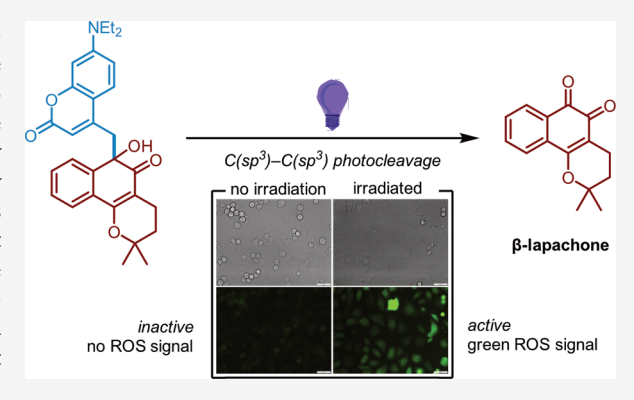
ACCESS I

III Metrics & More

Article Recommendations

s Supporting Information

ABSTRACT: β-Lapachone is an *ortho*-naphthoquinone natural product with significant antiproliferative activity but suffers from adverse systemic toxicity. The use of photoremovable protecting groups to covalently inactivate a substrate and then enable controllable release with light in a spatiotemporal manner is an attractive prodrug strategy to limit toxicity. However, visible light-activatable photocages are nearly exclusively enabled by linkages to nucleophilic functional sites such as alcohols, amines, thiols, phosphates, and sulfonates. Herein, we report covalent inactivation of the electrophilic quinone moiety of β-lapachone via a $C(sp^3)-C(sp^3)$ bond to a coumarin photocage. In contrast to β-lapachone, the designed prodrug remained intact in human whole blood and did not induce methemoglobinemia in the dark. Under light activation, the C-C bond cleaves to release the active quinone,



recovering its biological activity when evaluated against the enzyme NQO1 and human cancer cells. Investigations into this report of a $C(sp^3)-C(sp^3)$ photoinduced bond cleavage suggest a nontraditional, radical-based mechanism of release beginning with an initial charge-transfer excited state. Additionally, caging and release of the isomeric *para*-quinone, α -lapachone, are demonstrated. As such, we describe a photocaging strategy for the pair of quinones and report a unique light-induced cleavage of a C–C bond. We envision that this photocage strategy can be extended to quinones beyond β - and α -lapachone, thus expanding the chemical toolbox of photocaged compounds.

■ INTRODUCTION

Natural products serve important roles as leads in drug discovery with their unique biochemical activity and structural scaffold diversity. Bark of the lapacho tree (Tabebuia avellanedae) has been used for centuries in endemic traditional medicines, from which the isomeric natural products β -lapachone and α -lapachone, ortho- and para-naphthoquinones, respectively, have been isolated. Of the two quinones, β -lapachone has demonstrated significant antiproliferative, antibacterial, and antiviral activity.

Numerous studies have demonstrated β -lapachone antiproliferative activity against human cancers such as breast, ^{3,4} prostate, ^{5,6} pancreatic, ^{7,8} liver, ^{9,10} and lung. ^{11–13} With its p53-, ^{9,14} caspase-, ¹⁰ and cell cycle-independent cell death, ¹⁵ the broad-spectrum therapeutic ability of β -lapachone is attributed to its network of biological mechanisms that center around its redox cycling capability. Enzymes such as NAD(P) H quinone oxidoreductase-1 (NQO1) reduce β -lapachone to its corresponding hydroquinone that is unstable and spontaneously oxidizes, leading to large and rapid production of reactive oxygen species (ROS) (Figure 1). ¹⁶ The resulting ROS disrupts the integrity of the cell, causing DNA single strand breaks (SSBs), ¹⁷ loss of NAD(P)H and ATP pools, ¹⁸

and hyperactivation of polyADP-ribosepolymerase-1 (PARP-1), 13 ultimately causing programmed cell death downstream. 19

Although tissue sensitivity to β -lapachone is largely imparted by NQO1 levels—found up to 100-fold higher in cancerous tissue²⁰—clinical use in phase I and II trials has been greatly hampered by its systemic toxicity and poor pharmacokinetics.¹⁹ Namely, β -lapachone activity in red blood cells (RBCs) corresponds to the dose-limiting toxicity of methemoglobinemia and anemia.²¹ β -Lapachone is a promiscuous substrate for one- and two-electron oxidoreductases beyond NQO1, and its electrophilicity can enable it to directly react with critical cellular components.

To address toxicity due to nonspecific action of drugs, prodrug approaches have been developed to render a drug biologically inert until its activation. Traditional prodrug strategies typically involve internal stimuli, such as ROS, pH,

Received: January 11, 2023 Published: June 2, 2023





β-lapachone
$$H^+ + O_2^-$$

$$O_2$$

$$O_2$$

$$O_2$$

$$O_2^- + H^+$$
Seminquinone

Figure 1. Futile redox cycling of β-lapachone by NQO1. Direct one-electron reduction to the semiquinone can also occur by enzymes such as cytochrome b5 reductase.

or enzymes, and have recently been evaluated for β -lapachone. ^{22,23} The use of photoremovable protecting groups ("photocages") as a prodrug strategy offers unique advantages with light as an external stimulus for drug activation with high spatiotemporal control. Besides applications in therapeutics, photocages enable controlled release of substrates for time-resolved biological investigations in protein regulation, ^{24–26} cell signaling, ^{27,28} structure, ^{29,30} and optogenetics. ³¹

Various ultraviolet (UV) light-absorbing photocage classes have been developed, including phenacyl, benzoinyl, and the popular *ortho*-nitrobenzyl structures. More recently, several groups have introduced coumarins, so quinolines, and boron-dipyrromethenes aphotocages that exhibit the key advantage of high molar absorptivity in the visible light range as to avoid UV light-associated cytotoxicity in biological systems. In particular, coumarins are popular chromophores with their tunable spectral properties and ease of synthetic accessibility.

Substrates are nearly exclusively covalently linked to photocages via functional sites that are key to its activity, often through alcohol, amine, thiol, phosphate, or sulfonate groups. However, photorelease efficiency is highly dependent on leaving group stability, demanding low pKa values of the conjugate acid. As such, alcohols and amines are routinely linked via carbonate and carbamate linkages that undergo decarboxylation after photorelease. In contrast, inactivation by functionalizing electrophilic sites, such as *ortho-* and *para*-quinones, is an immense challenge in the development and use of photocages. Enabling such a strategy would open the chemical space of caged compounds for more diverse biological applications and studies.

In this work, we report the design, investigation, and evaluation of a small molecule, photocaged β -lapachone prodrug. Conversion of the *ortho*-quinone to an α -hydroxyketone bound to a coumarin photocage via a $C(sp^3)-C(sp^3)$ bond consequently renders the site inactive to redox cycling. Upon light activation, the C–C bond cleaves to release β -lapachone, restoring its biological activity in vitro and in cellulo. Mechanisms of the unusual $C(sp^3)-C(sp^3)$ bond cleavage were investigated and extended for release of the *para*-quinone, α -lapachone, from a derivatized γ -hydroxyketone. The light-activated prodrug approach enables the delivery of a more stable, nontoxic agent, where β -lapachone can be

activated with high spatiotemporal control under cellular conditions.

■ RESULTS AND DISCUSSION

Synthesis of Photocaged β -Lapachone. To mask β -lapachone activity, we sought to remove its characteristic electron-accepting property that is central to its network of biological mechanisms. We envisioned modification of a carbonyl of the quinone with the popular coumarin photocage, 7-diethylaminocoumarin-4-methyl (DEACM). As such, a three-step, one-pot synthesis was developed to achieve reductive coupling between β -lapachone and DEACM, synthesizing key prodrug, compound 1 (Scheme 1).

Scheme 1. One-Pot Conditions for Synthesis of 1 and Coumarin Derivatives

The alkylbromide coumarin precursor of DEACM, 7-diethylamino-4-coumarinyl bromide (DEACM-Br), was prepared accordingly from literature protocols to be utilized for coupling. Briefly, SeO₂-mediated benzylic oxidation of commercially available DEACM (CM1) afforded the corresponding aldehyde (CM2). Reduction with NaBH₄ to the

Table 1. Photophysical Properties of Compound 1 and Other Coumarins

	$\lambda_{\rm ex}$ (nm) (MeOH/PBS)	λ_{em} (nm) (MeOH/PBS)	$\Phi_{\rm f}$ (MeOH)	$\varepsilon \times 10^3 (\mathrm{M}^{-1}\mathrm{cm}^{-1})^a$	Φ_{r} (%)	$\varepsilon \; \Phi_{r} \; (M^{-1}cm^{-1})$		
compound 1	391/407		< 0.0001	26	0.35	91		
CM1	375/380	437/469	0.73 ^b	30.7				
CM2	385/395	449/501	0.31 ± 0.05	11.2				
CM3	370/380	453/499	0.37 ± 0.04	19.5				
^a Determined in dimethyl sulfoxide (DMSO). ^b Reported in ethanol by Jones et al. ⁴³								

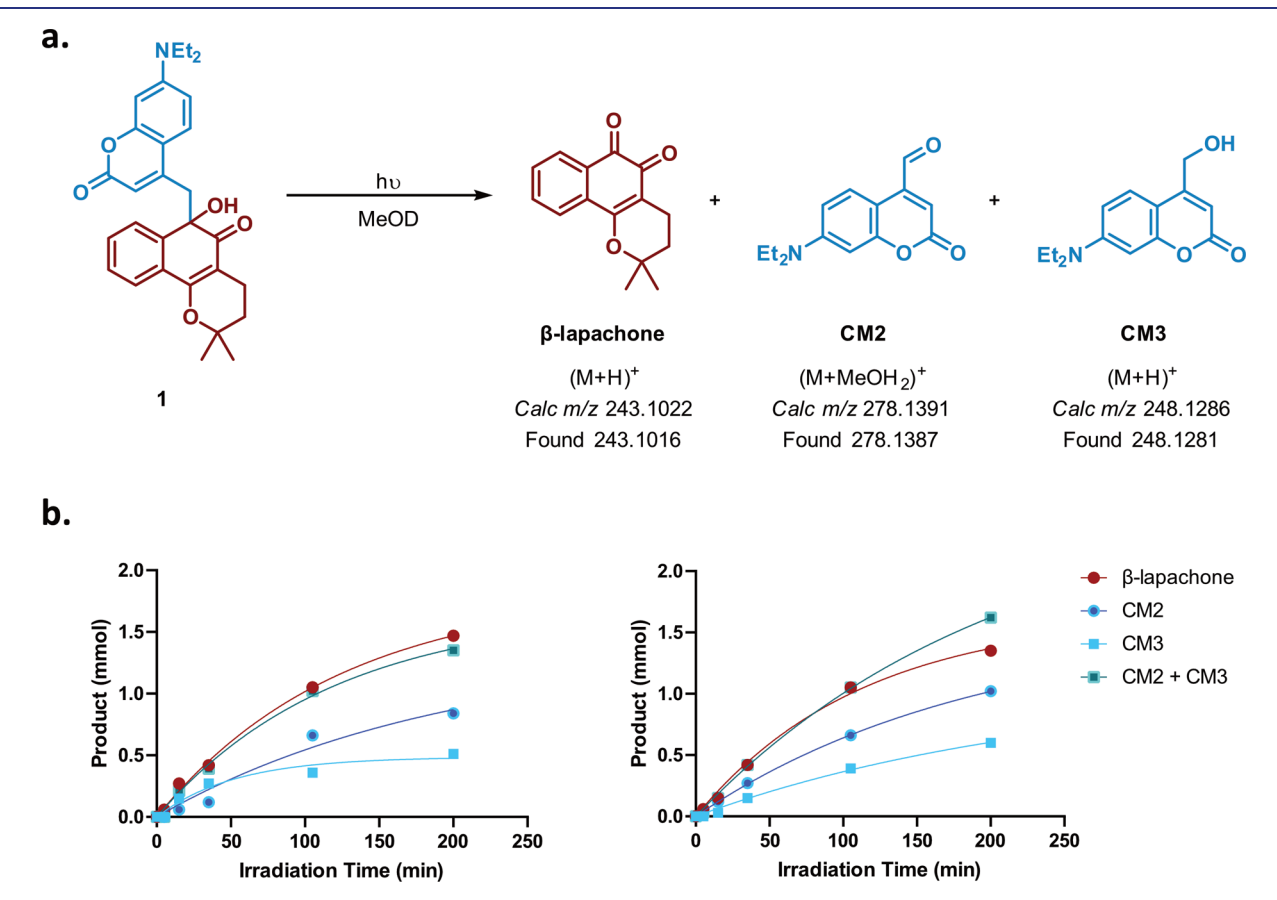


Figure 2. (a) 1 lysis under 365 irradiation into β-lapachone, CM2, and CM3 in MeOD. Products were identified by 1 H NMR in comparison to standard samples and HRMS. (b) Release of products from lysis of 1 under 365 irradiation over time under either O_2 or Ar conditions, monitored by qNMR.

alcohol (CM3), followed by PBr₃ bromination, afforded DEACM-Br (Scheme S1).

All three steps of the one-pot synthesis of 1 were conducted at room temperature. In the first step, sodium dithionite reduces the benzylic ketone of the quinone moiety. Subsequent treatment with base in the second step promotes formation of a nucleophilic enolate that, in the third step, undergoes a substitution reaction with the added electrophile. Soft electrophile DEACM-Br afforded the chiral, C-modified 1 in satisfactory yields of 68%.

Indications that 1 was chiral were noted in the 1 H NMR spectrum that showed unique diastereotopic proton signals, further confirmed by separation of the enantiomers by chiral high-performance liquid chromatography (HPLC). While unclear by 2D NMR studies, single-crystal X-ray diffraction indicated that β -lapachone was modified with the coumarin at its benzylic ketone carbon (see Section S10). While α -hydroxyketones from 1,2-diones are typically formed using harsh Grignard or organolithium reagents, which require exclusion of moisture and oxygen, the one-pot synthesis

developed for 1 enables selective modification under less stringent conditions.

Photochemical Release of *β***-Lapachone.** Since *β*-lapachone has not been photocaged previously, the photophysical properties of **1** were compared to other substituted coumarins, **CM1**, **CM2**, and **CM3**. **1** possesses a broad visible light-absorbing band with maximal absorption at 391 nm $(26,000 \text{ M}^{-1} \text{ cm}^{-1})$ in MeOH that red-shifts 16 nm in phosphate-buffered saline [PBS (pH 7.4)] to 407 nm. The absorbance of **1** is the most-redshifted and undergoes the largest bathochromic shift between organic to aqueous solvent in comparison to the other coumarins (Table 1). In methanolic solution, **1** strikingly displays negligible fluorescence, which contrasts the otherwise high-fluorescence quantum yields of the other coumarins (0.31-0.73) (Table 1).

Photocleavage of $C(sp^3)-C(sp^3)$ bonds in photocages has not been as developed as C-heteroatom linkages. We first analyzed photochemical release of β -lapachone from 1 via direct ¹H NMR quantitative analysis using 1,3,5-trimethoxybenzene as an internal standard. A solution of 1 in anhydrous

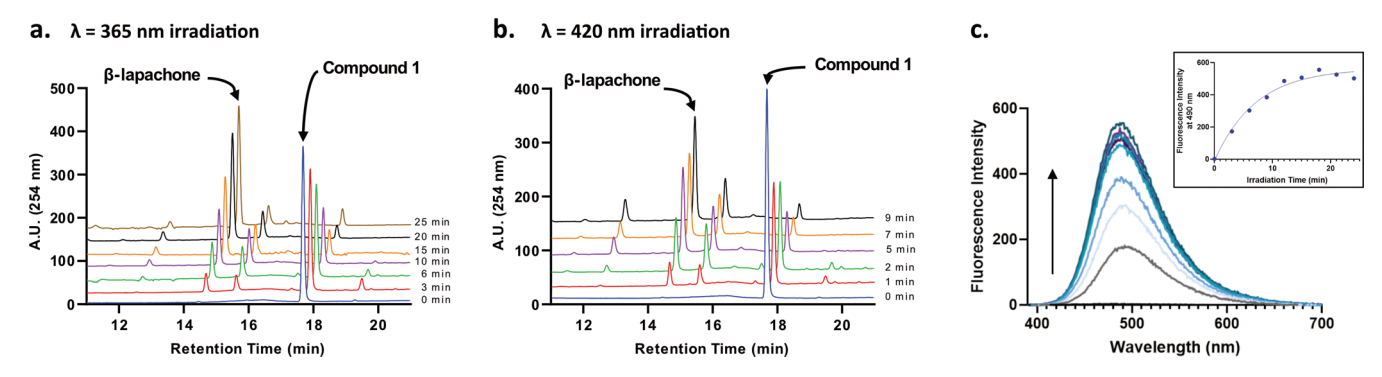


Figure 3. Monitoring of β-lapachone release from a 100 μM solution of 1 in PBS (pH 7.4, 1% DMSO) under (a) 365 or (b) 420 nm irradiation. AUC analysis was conducted by use of standard curves. (c) Fluorescence monitoring of a 20 μM solution of 1 under 365 nm irradiation. At given time points, the solution was excited at 385 nm and increasing maximal fluorescence was observed at 490 nm.

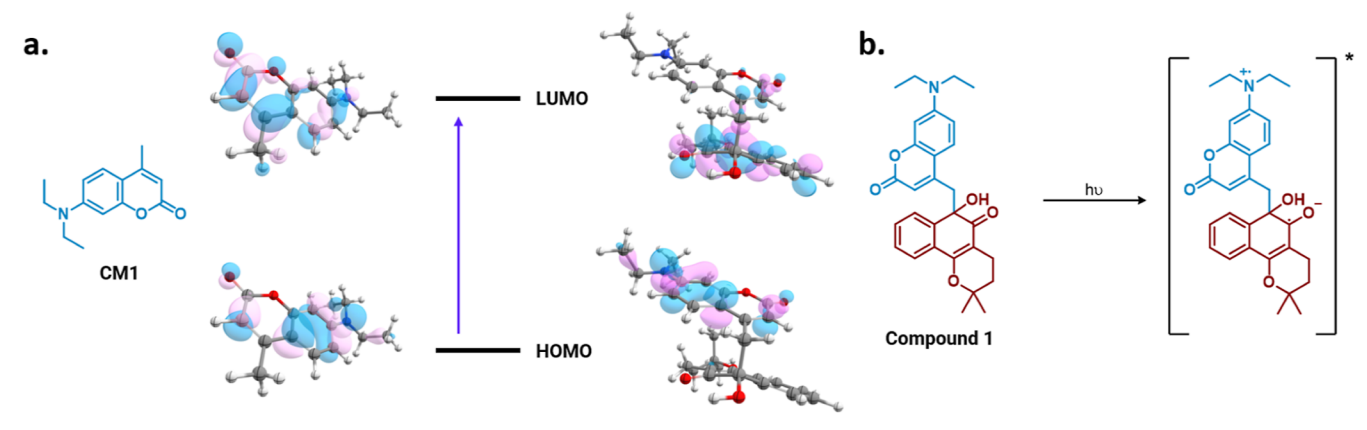


Figure 4. (a) Computed HOMOs and LUMOs of CM1 (left) and 1 (right). (b) Suggested biradical excited internal charge-transfer state of 1 supported by change in Mulliken charges.

MeOD (5 mM) was subjected to 365 nm irradiation (51 mW/ cm² lamp), and its ¹H NMR spectrum was monitored over time. With irradiation, 1 converted into β -lapachone and two coumarin species, CM2 and CM3 (Figure 2a), indicating cleavage of the benzylic coumarin photocage. Products were identified by comparison of the ¹H NMR spectrum with pure standard samples of β -lapachone, CM1, CM2, and CM3 (Figures S3-S5). The products of irradiated 1 were further confirmed by reverse-phase HPLC separation and subsequent high-resolution mass spectrometry (Figure 2a). The quantum yield of β -lapachone release from 1 in MeOH was determined to be 0.35% under 365 nm irradiation ($\varepsilon \Phi = 91 \text{ M}^{-1} \text{ cm}^{-1}$) by ferrioxalate actinometry (Table 1). Since oxidized products were identified, comparison of photolysis rates of 1 and the products formed was assessed under oxygenated and inert, degassed conditions. An anhydrous solution of 1 in MeOD was bubbled with oxygen, while a separate solution was prepared under inert conditions, degassed (three freeze-pump-thaw cycles), and kept under argon in a sealed J-Young tube. Interestingly, no difference in the rate nor identity of products formed was observed between the two conditions (Figure 2b). In both cases, the combined concentration of CM2 and CM3 formed equaled β -lapachone in a 1:1 mole ratio. Lack of oxygen influence suggests that lysis of 1 likely occurs from the excited singlet state (S_1) (in agreement with previous analysis of coumarin photocages), rather than a triplet excited state that can be easily quenched by oxygen.⁴⁴

To assess the applicability of β -lapachone release in biological systems, a 100 μ M solution of 1 in PBS (pH 7.4)

containing 1% DMSO was irradiated and monitored by analytical HPLC. We studied the lysis under both 365 nm (51 mW/cm²) and 420 nm (30 mW/cm²) light, the latter of which is more appropriate for biological applications as it minimizes absorption by endogenous chromophores. As displayed in Figure 3a,b, with increasing irradiation time, the disappearance of the compound 1 peak corresponded to the concomitant increase of a β -lapachone peak, identified by matching retention time (14.488 min) and absorption spectrum of pure β -lapachone standard. ⁴⁵ A plot of the decomposition of 1 to β -lapachone over the irradiation time was calculated by area under the curve (AUC) analysis, revealing first-order decay of 1 with a rate of $k_{\rm decay} = 1.606 \times 10^{-3} \text{ s}^{-1}$ and $k_{\rm decay} = 6.806 \times 10^{-3} \text{ s}^{-1}$ under 365 and 420 nm irradiation, respectively (Figure S13). To complement this experiment, we indirectly monitored photolysis via fluorescence since 1 is nonfluorescent whereas CM2 and CM3 are (Table 1). The coumarin byproducts absorb broadly around 385 nm, which was the wavelength used to excite a 20 μM solution of 1 in PBS preexposed to 365 nm lamp irradiation at various time points. Fluorescence of the solution dramatically increased maximally at 490 nm as 1 converted to the corresponding coumarins (Figure 3c).

Computational Investigation. Considering the nature of the C–C bond being photocleaved, we investigated the mechanism of uncaging of 1. A single example of a C–N bond cleavage from 4-methylcoumarins reported by Schoenleber and Giese determined cleavage to be induced from an internal charge-transfer state. We turned to 1 and noted the lack of

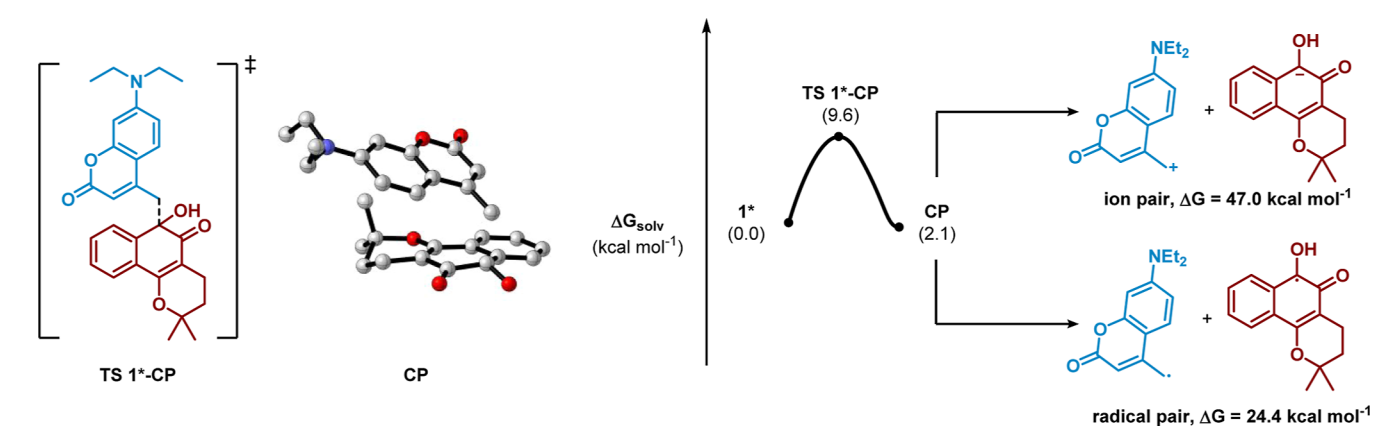


Figure 5. Free energy profile of the C-C bond cleavage step after excitation of 1 obtained at the M06-2x(D3)/aug-cc-pvtz/SMD = H_2O level of theory. The key transition state depicting the $C(sp^3)-C(sp^3)$ bond undergoing scission and the resulting contact pair is depicted on the left. The thermodynamics of the intermediate diffusing to form a solvent-separated ion pair or radical pair was evaluated at the same level of theory.

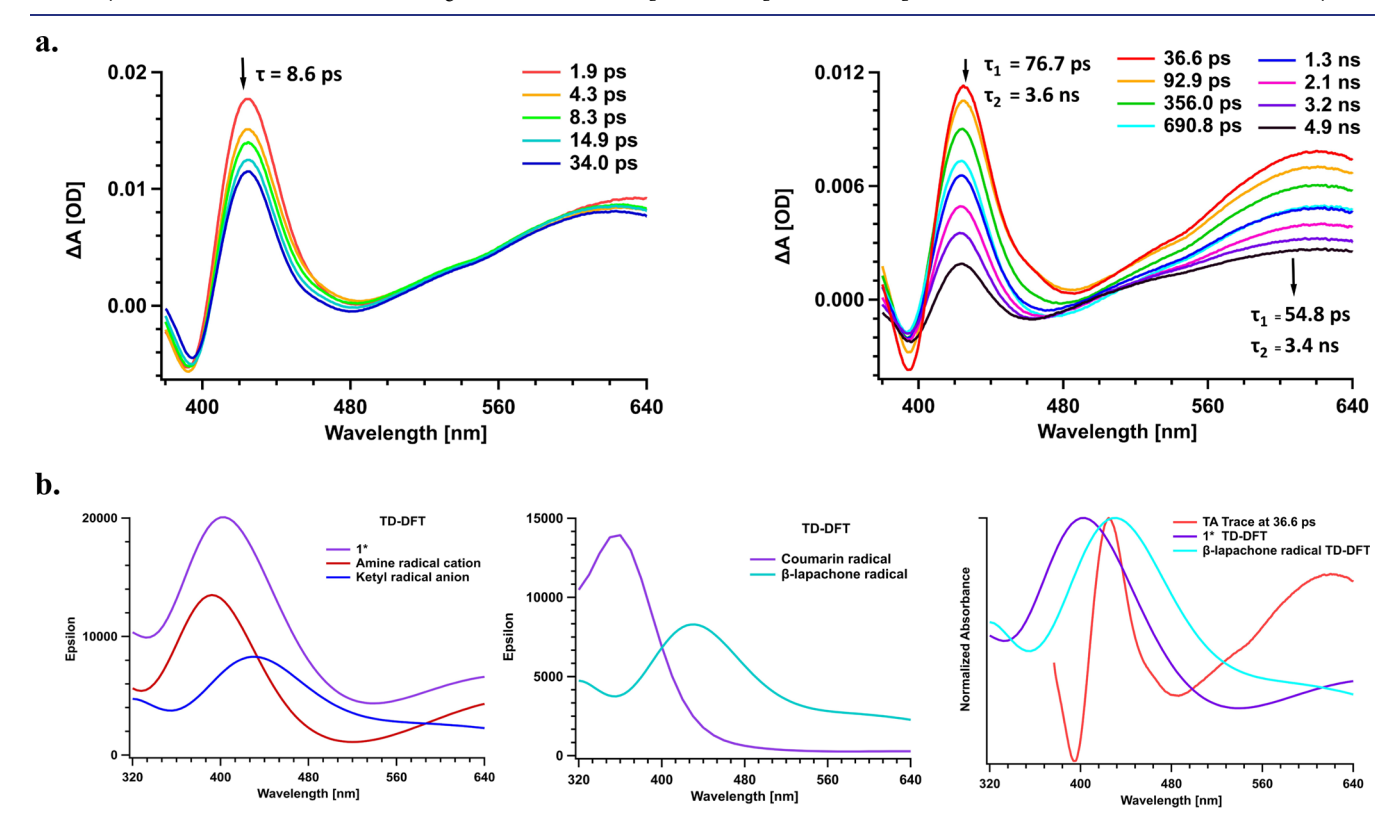


Figure 6. (a) fs-TA of 1 after 365 nm excitation in acetonitrile recorded within 100 ps and 5 ns. (b) Comparison of experimental TA spectra obtained at 36.6 ps after 365 nm excitation in acetonitrile with TD-DFT spectra of 1*, coumarin, and β -lapachone radical obtained at the PBE0//B3LYP/6-31G(d,p)/SMD = acetonitrile (note: experimental TA spectra are shown between 380 and 640 nm, whereas TD-DFT spectra are shown between 320 and 640 nm).

fluorescence properties, which can suggest an intramolecular charge transfer upon excitation, whereby fluorescence relaxation from coumarin is blocked.

We utilized density functional theory (DFT) and time-dependent DFT (TD-DFT) to investigate the possibility of an internal charge-transfer event. The S_0 and S_1 states of 1 and unsubstituted CM1 were compared. The highest occupied molecular orbital (HOMO) and lowest unoccupied molecular orbital (LUMO) of CM1 were both found to be localized along the coumarin π -system, whereas a spatial separation between the two was observed for 1 (Figure 4). In 1, the HOMO is also localized along the coumarin. However, the

LUMO is localized predominantly along the lapachone-derivatized structure, instead of the lactone as observed in CM1. Mulliken charge analysis indicated that the nitrogen atom on the coumarin becomes more positive in the S_1 state, while the carbonyl carbon of the α -hydroxyketone displayed more negative character, when compared to the S_0 state. These computational results suggest that upon irradiation, a charge transfer from nitrogen to carbon can occur to form a biradical excited-state species containing an amine radical cation and ketyl radical, consistent with previous reports (Figure 4). 46

DFT calculations were carried out to investigate the energetics of the C-C bond cleavage. Initially, 1 is excited

to the S_1 state (1*) following irradiation. 1* undergoes a scission of the $C(sp^3)-C(sp^3)$ bond with an energy barrier of 9.6 kcal mol⁻¹ to form a contact pair, CP (Figure 5). This result is consistent with barriers for uncaging of other coumarin-based photocages.⁴⁷ At this point, the exact identity of the pair that results from C-C bond cleavage is unclear, resulting from either homolysis of the bond to give a radical pair or heterolysis to give an ion pair. We evaluated the thermodynamics of the contact pair diffusing to a solventseparated ion pair or a radical pair. The calculations found that both processes were endergonic. Interestingly, the diffused radical pair was found to be far more thermodynamically stable $(\Delta G = 24.4 \text{ kcal mol}^{-1})$ than the solvent-separated ion pair $(\Delta G = 47.0 \text{ kcal mol}^{-1})$. Considering most uncaging processes involving coumarins occur via a heterolysis mechanism, these results prompted us to investigate a radical-mediated bond cleavage.

Transient Absorption Profile of 1. To probe the nature of the excited state (1*) and possible coumarin radical or other intermediate species that would arise from bond cleavage of 1, transient absorption (TA) spectra of 1 in acetonitrile were obtained using a 365 nm pump laser beam, as depicted in Figure 6a. A control TA study with CM1 was also performed using the same 365 nm pump laser beam in acetonitrile (see the Supporting Information) to provide a reference spectrum for comparison of the localized coumarin excited state. For the control experiment, our experimental findings matched the report by Wen and Yip et al., who investigated the TA profile of CM1 in methanol. 48 A strong bleaching and weak growth was observed with a clear isosbestic point at 550 nm. They concluded that the bleaching occurs due to stimulated emission and the growths were from formation of an excited internal charge-transfer state, both with a lifetime of 2.25 ns. 48

TA studies of 1 showed fast kinetic processes below 2 ps (Table 2). Namely, bleaching was observed between 430 and 500 nm and growths in absorption observed between 320-420 and 630-725 nm. Between 35 ps and 5 ns timescales, we observed a broad decay between 400 and 640 nm. Kinetic traces obtained at 424 and 620 nm were both fitted with biexponential decays with lifetimes of 77 ps, 3.6 ns (at 424 nm) and 55 ps and 3.4 ns (at 620 nm), respectively. Hence, we predicted that the broad absorption was due to two species, a short-lived species having a lifetime of 50-80 ps and a longerlived species of lifetime 3.4-3.6 ns. Changes in the TA were analyzed for possible charge-transfer state and other radicals. While normally singlet excited-state absorptions cannot be predicted by TD-DFT, a charge-transfer state should consist of a coumarin cation radical and lapachone anion radical. Assuming that the two radical ions are noninteracting, the absorption spectrum can then be predicted as the sum of the TD-DFT-predicted absorptions for the isolated radical ions. The predicted absorption spectra of 1*, coumarin radical, and β -lapachone radicals were calculated by PBE0/6-31G(d,p) using the SMD solvation model in acetonitrile, where the coumarin radical (Figure 6) was calculated to possess a strong absorption band at 340 nm (Figure S20). The sum of the absorptions for 1^* and the corresponding β -lapachone radical matches well with the TA profile at short times, both having a broad absorption between 320 and 640 nm. Therefore, we assign the shorter-lived species with a lifetime between 50 and 80 ps to be 1*. The longer-lived nanosecond species has an absorption spectrum consistent with the β -lapachone radical.

Table 2. Lifetimes of TA of Compound 1 Events

delay time	event	event	event
<2 ps	growth 320-430 nm (226-252 fs)	bleaching 430-500 nm	growth 630– 725 nm
2- 100 ps	growth 320– 390 nm (5.52 ps)	decay 390-430 nm (8.6 ps)	decay 600- 725 nm (45.1 ps)
35 ps- 5 ns	decay 320- 360 nm (2.47 ns)	decay 390-725 nm (54.8 ps -76.7 ps), (3.4. ns-3.6 ns)	

EPR Radical Detection. Electron paramagnetic resonance (EPR) spectroscopy was employed to directly detect any radical intermediates arising from lysis of **1**. A 5 mM solution of **1** in anhydrous MeOH was prepared in an air-free environment and sealed to preclude any oxygen in the sample. As the sample was irradiated with 365 nm light (ex situ of the magnet), a build-up of a radical signal with a quintet hyperfine splitting pattern was observed in the EPR spectra recorded at 292 K (Figure 7). The build-up of the signal over the

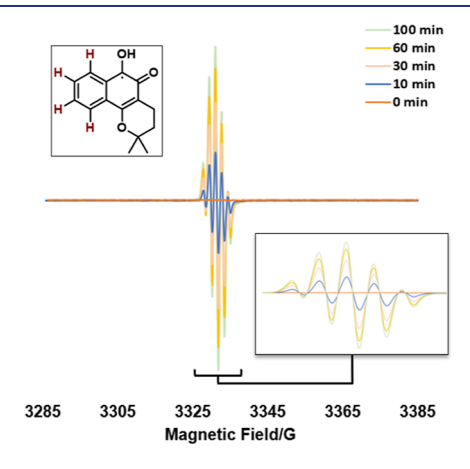


Figure 7. EPR spectra of **1** under 365 nm light irradiation (5 mM in MeOH). Inset shows a quintet hyperfine splitting and increase of signal intensity over irradiation time.

irradiation time indicated a long lifetime, suggesting high stability of the radical. Quintet hyperfine splitting implied that the unpaired electron could interact with 4 equiv spin-active nuclei, which we assign to be the four hydrogens along the delocalized aromatic ring of β -lapachone. The splitting pattern exactly matches a report by Villamil et al. that detected the semiquinone radical signal of a β -lapachone derivative reduced in microsome fractions, ⁴⁹ supporting the proposed β -lapachone radical shown in Figure 5.

With the information provided by laser flash photolysis and EPR, a possible mechanism for the C–C bond cleavage is shown in Scheme 2. Excitation of 1 leads to a biradical species in the S_1 state. Collapse of the ketyl radical leads to cleavage of the C–C bond in a process similar to the cleavage observed by Giese et al. to form the coumarin radical and β -lapachone radical. We hypothesize that the propensity of the coumarin to accept electron density facilitates this process. From the β -lapachone radical intermediate, we propose that β -lapachone can form either via direct oxidation by air or from hydrogen atom abstraction from solvent. However, it is unclear how oxidized coumarin products, CM1 and CM2, are formed from the coumarin radical under a degassed, light-irradiated solution

Scheme 2. Proposed Mechanism of Cleavage of 1

of 1 (Figure 2), but an intermolecular redox reaction could be involved.

Leaving Group Dependency. To evaluate the importance of the α -hydroxyketone on photo-uncaging efficiency, we sought to prepare an O-functionalized derivative of 1. We subjected β -lapachone to the one-pot conditions, utilizing a hard electrophile, Ac_2O , to afford the achiral O-modified 2 in 45% yield as a single regioisomer, assigned based on 1D and 2D NMR studies (Scheme 3). ${}^1H-{}^1H$ nuclear Overhauser

Scheme 3. Synthesis of Compound 3

effects were observed between the acetate and the napthoquinone ring and between the hydroxyl and pyran ring. ⁵⁰ 2 was converted into the photocaged compound 3 by treatment with base and DEACM-Br.

The computed HOMO to LUMO transition of 3 showed a similar pattern to 1, with no contribution of the acetate in the LUMO (Figure S15). However, we observed that 3 does not undergo C–C bond cleavage to release a corresponding 2 lapachone core and coumarin byproducts. Instead, when a solution of 3 in anhydrous MeOD (5 mM) under 365 nm irradiation was monitored by ^1H qNMR, an intact, rearranged product was observed. Once produced, this product exhibited high photostability with no change in the NMR spectrum under further irradiation (Figures S14 and S17). The lack of photo-uncaging of 3 suggests that the α -hydroxyketone is important for photoconversion of 1 to β -lapachone.

Extension to *para***-Quinones.** After our assessment of photorelease of the *ortho*-quinone, β -lapachone, from 1, we set out to assess applicability of coumarin photorelease of the *para*-quinone, α -lapachone. *Para*-quinones are highly valuable structures in drug development, found in many clinically relevant drugs such as doxorubicin, mitoxantrone, and mitomycin C. Many *para*-quinone natural products suffer

from adverse toxicity that has blocked their use as chemotherapeutics, such as streptonigrin, 52 that may instead become more clinically useful with an applied photocage prodrug strategy.

We subjected α -lapachone to the one-pot conditions employed for β -lapachone to assess the applicability of single-carbonyl modification to 1,4-diones. The reaction yielded the corresponding C-modified, γ -hydroxyketone, 4 (Scheme 4). Compared to 1, 4 was formed in a much lower

Scheme 4. Synthesis of Caged α -Lapachone, 4

yield (15%) with unreacted α -lapachone largely recovered. Nevertheless, the product was produced in a regioselective manner with modification at the carbonyl ortho to the pyran oxygen, confirmed by X-ray crystallography.

We applied computational analysis of the S_0 to S_1 transition of 4 (Figure 8) and observed similar spatial separation in the HOMO and LUMO as observed with 1 and 3. The computed

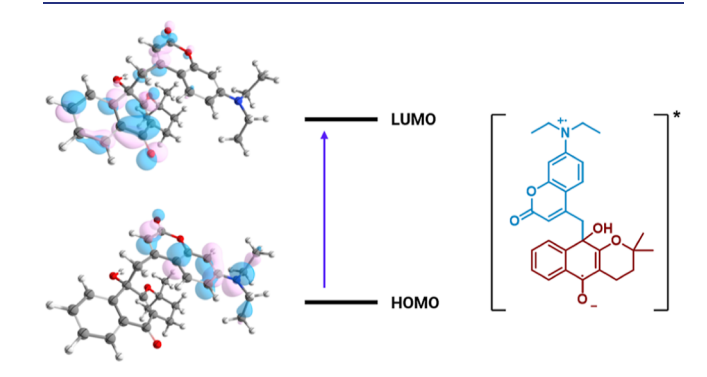


Figure 8. (a) HOMO to LUMO transition of **4.** (b) Suggested biradical excited internal charge-transfer state analogous to **1**.

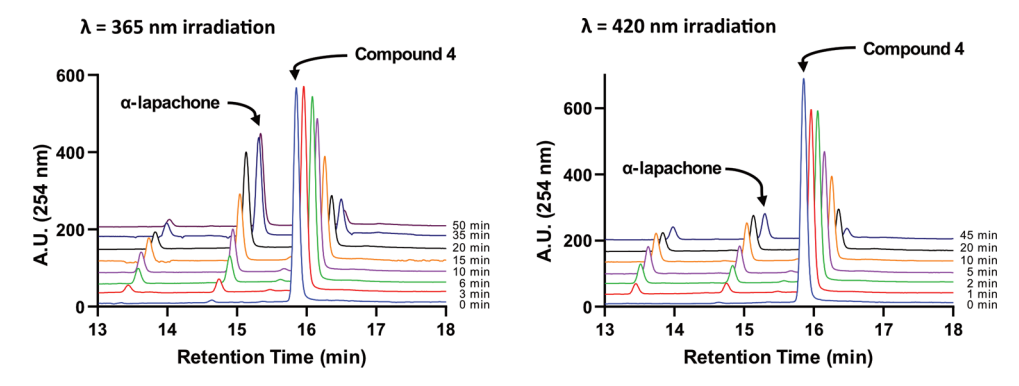


Figure 9. HPLC monitoring of release of a 100 μ M solution of α-lapachone from 4 with 365 and 420 nm irradiation in PBS (pH 7.4, 1% DMSO).

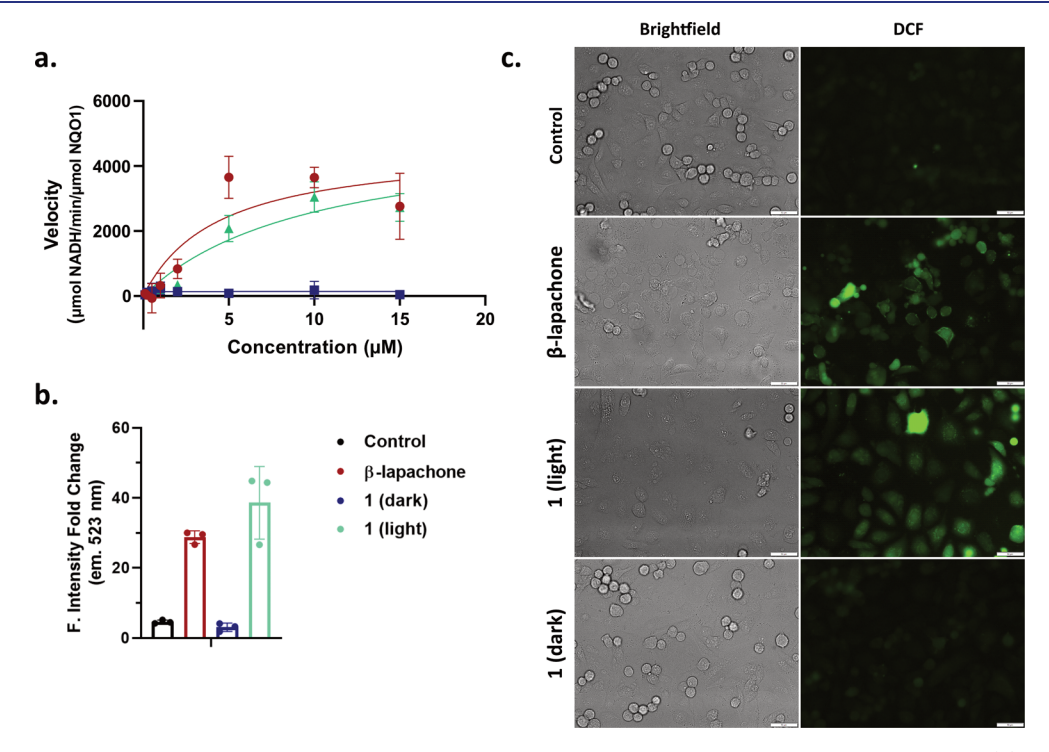


Figure 10. (a) NQO1 Michaelis—Menten curves of β -lapachone and 1 with or without pretreatment of 365 nm irradiation. (b) In vitro monitoring of DCF fluorescence from oxidation by ROS from NQO1 redox cycling of β -lapachone or 1 in the dark or pretreated with 365 nm light. (c) Fluorescence imaging of intracellular ROS production in A549 lung carcinoma cells treated with β -lapachone, 1 (with or without 420 nm light), or vehicle (DMSO). Without light irradiation, minimal DCF fluorescence was observed in cells treated with 1 (bottom row). In cells treated with β -lapachone or 1 with light (420 nm, 7 min, 12.7 J/cm²) during incubation, DCF fluorescence was observed, indicative of ROS production (middle rows). 20× magnification, scale bars = 50 μ m.

HOMO was localized along the coumarin π -system, and the LUMO localized along the derivatized α -lapachone (Figure 8). With our analysis, we proposed a similar internal charge-transfer excited state for 4 that contains the amine radical cation and ketyl radical that can ultimately induce C–C bond cleavage to produce an α -lapachone radical in an analogous pathway suggested for 1.

The ability of the coumarin cage to cleave a C–C bond to restore a *para*-quinone was evaluated with 4 by 1 H qNMR. A solution of 4 in anhydrous MeOD (5 mM) irradiated with 365 nm light displayed the formation of characteristic α -lapachone peaks, as well as the same CM2 and CM3 byproducts observed for photo-uncaging of 1 (Figure S7).

HPLC analysis of 4 followed by 365 and 420 nm irradiation was performed under the same conditions used for 1 (Figure 9). 4 showed slower kinetics of release than 1 ($k_{\rm decay} = 8.452 \times 10^{-4} \, {\rm s}^{-1}$ for 4 vs $k_{\rm decay} = 1.606 \times 10^{-3} \, {\rm s}^{-1}$ for 1 under 365 nm)

 $(k_{\rm decay}=1.193\times 10^{-3}~{\rm s^{-1}}$ for 4 vs $k_{\rm decay}=6.806\times 10^{-3}~{\rm s^{-1}}$ for 1 under 420 nm) (Figure S13). The slower kinetics could be due to differential stability of the radical semiquinone leaving group. Although α -lapachone does not possess NQO1 redox cycling activity like β -lapachone, the photocaging/uncaging strategy opens future possibilities of photocaging *para*-quinones that have biological activity.

Compound 1 Loss of Activity and Recovery with Light. NQO1 has been largely studied as the key enzyme responsible for β -lapachone redox cycling. With loss of the diketone moiety in 1, we anticipated 1 to be NQO1 inactive. To assess NQO1 activity, β -lapachone and 1 were incubated with NQO1, NADH, and bovine serum albumin. The consumption of NADH to NAD⁺ cofactor was monitored by its characteristic loss of absorbance at 340 nm. 1 showed negligible NQO1 activity; however, preirradiated samples (365 nm light) prior to incubation displayed NADH consumption

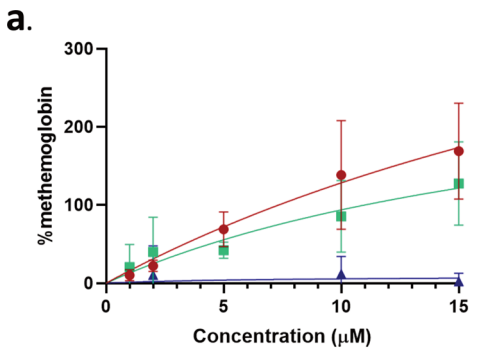
rates similar to standard β -lapachone samples (Figure 10a). Over the time course, more than one equiv of NADH was consumed if incubated with β -lapachone or 1 with light, demonstrating turnover consistent with the redox cycling mechanism (Figure 1).

ROS is the major cytotoxic product of the rapid redox cycling of β -lapachone, and so the ability to control its production with light activation of 1 was evaluated. To monitor ROS production, we employed the commercially available ROS sensor, 2',7'-dichlorofluorescein (DCFH₂). Samples of β -lapachone, 1 (dark or preirradiated with 365 nm lamp), or vehicle alone (DMSO), were prepared and incubated with NADH and NQO1 but with the addition of DCFH₂ (Figure 10b). In agreement with the NQO1 activity assay, a 10 min NQO1 incubation with 1 displayed negligible DCF fluorescence when compared to the control of vehicle alone with or without light. However, if samples were pretreated with light to induce β -lapachone release, after the 10 min incubation period, strong DCF green fluorescence signals were observed with similar intensities when using a β lapachone standard.

The light-controlled ROS production was evaluated in A549 cells treated under various conditions of β -lapachone, 1 (with or without light), or vehicle alone, with a cell permeable diacetate derivative, 2',7'-dichlorofluorescein diacetate (DCFH₂-DA) ROS sensor (Figure 10c). A549 cells coincubated with β -lapachone and DCFH₂-DA for 20 min displayed typical DCF signals from the rapid redox cycling. However, only in cells incubated with 1 for 10 min with subsequent 420 nm light (7 min, 12.6 J/cm²) irradiation and then coincubated with the addition of DCFH2-DA for 20 min were green DCF fluorescence signals observed. Incubated 1 samples that were not activated with light displayed no fluorescence.

Major obstacles in the administration of β -lapachone in the clinic consist of its rapid renal clearance and observed methemoglobinemia. The short systemic half-life of β lapachone can be attributed to the highly reactive nature of the diketone moiety that renders it prone to extensive metabolism in RBCs.53 We tested 1 in human whole blood samples and observed no decrease in concentration after a total incubation time of 2 h (see Table S1). Conversely, β lapachone was quickly consumed with a determined half-life of 19.86 min, in agreement with literature reports⁵⁴ (see Table S2). Thus, conversion of the quinone to an α -hydroxyketone successfully removed the reactive nature of the site that is otherwise prone to undesirable enzymatic reactions.

Methemoglobin formation in RBCs with β -lapachone treatment is largely attributed to the presence and redox cycling of β -lapachone by one-electron oxidoreductases such as cytochrome b5r. 21 Compound 1 was tested for its ability to block activity on one-electron oxidoreductases and remain nontoxic to RBCs. RBCs were first isolated from human whole blood samples and then incubated for 2 h with β -lapachone, 1 (dark or pretreated with light), or vehicle alone. The cells were then lysed to release cellular components and analyzed for methemoglobin formation. Hemoglobin possesses two characteristic absorption peaks between 500 and 600 nm, while methemoglobin possesses poor absorbance in this range and instead shows a characteristic band at 630 nm. When compared to the control, β -lapachone induced dose-dependent formation of methemoglobin, which 1 also displayed if activated with light to release β -lapachone (Figure 11). In



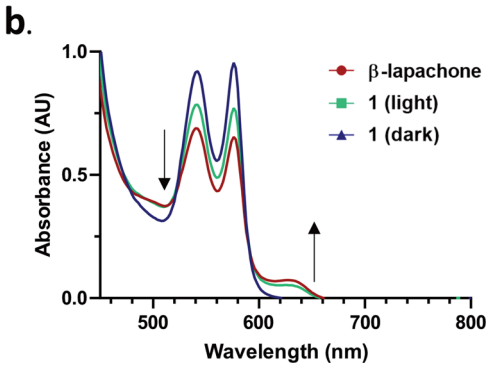


Figure 11. (a) Methemoglobin production in human RBCs incubated with β -lapachone or 1 (dark or preirradiated with light) (0–15 μ M) for 2 h. (b) Absorbance spectra of hemoglobin and methemoglobin in representative samples of blood incubated with 15 μ M of β -lapachone or 1 (with or without pretreatment of light). Oxidation of hemoglobin into methemoglobin is indicative by decrease in absorbance at 500-600 nm and an absorbance increase at 630 nm.

contrast, 1 in the dark did not induce any methemoglobin formation across the tested concentration range $(0-15 \mu M)$, indicating that the design can mitigate blood-related systemic

The effectiveness of 1 to block the broad spectrum of β lapachone cytotoxicity and its ability to recover its potency with photoactivation were determined in seven different cancer cell lines; A549, H596, MCF7, MDA-MB-231, Capan2, PANC-1, and Hep G2. Cells were treated with β -lapachone or 1 (0-32 μ M), then either left to incubate for 24 h (dark condition) or, after an initial 1 h of incubation, irradiated with light (420 nm, 7 min, 12.7 J/cm²) and then incubated again for 23 h (light condition). After the incubation periods, cell death was assessed by the standard 3-(4,5-dimethylthiazol-2-yl)-2,5diphenyl-2H-tetrazolium bromide assay. As summarized in Figure 12, administration of 1 was able to mitigate toxicity observed with β -lapachone. In cells with 1, but treated with light, potent EC50 values in the micromolar range were then observed, indicating its photocytotoxic behavior (see Table S3 for phototherapeutic indexes). The potency is slightly decreased from native β -lapachone, which is expected since the photorelease is not quantitative as noted in the HPLC monitoring experiment. As a control, cells treated with both β lapachone and light (420 nm) exhibited negligible difference in cytotoxicity from cells treated with β -lapachone alone, indicating no gain or loss of activity with the light dose employed.

Both MDA-MB-231 and H596 cell lines are reported to lack NQO1 that would otherwise mediate β -lapachone redox cycling. However, these two cell lines still responded to β -

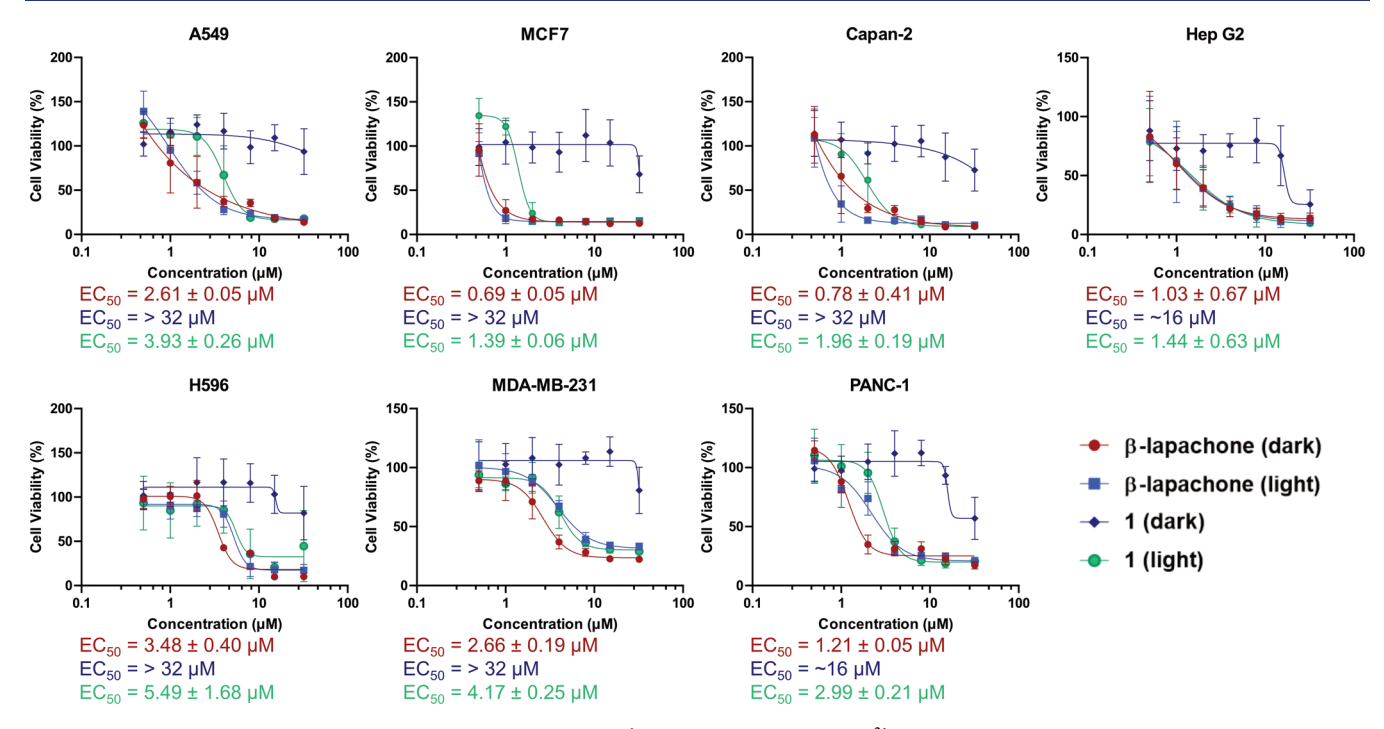


Figure 12. Cell viability of 1 in the dark or with light irradiation (420 nm, 7 min, 12.7 J/cm²) compared to β -lapachone against a panel of human cancer cell lines. Cells were treated with increasing concentrations (0–32 μM) of respective compounds, with treatment by 1 with light-restoring dose-dependent response in viability like β -lapachone. Data are presented as mean \pm SD (n = 9).

lapachone with EC₅₀ values in the micromolar range. β -Lapachone is not exclusive to NQO1 but rather a promiscuous substrate for many other oxidoreductases that may be responsible for the cell death observed. Different oxidoreductases are expressed in different levels across different tissue types; thus, the ability of 1 to mitigate cytotoxicity against the various cell lines demonstrated a strong increase in the applicable therapeutic window of our prodrug photocaged strategy.

CONCLUSIONS

In this study, we evaluated a prodrug design of the *ortho*-quinone natural product, β -lapachone, by conversion of the diketone to an α -hydroxyketone. The design renders β -lapachone biologically inactive, completely blocking NQO1 redox cycling and ROS production, methemoglobin formation, and mitigated cytotoxicity in various human cancer cell lines. When the coumarin photocage covalently attached to the hydroxyketone via a $C(sp^3)-C(sp^3)$ bond, light activation released β -lapachone, regaining its biological anticancer activity compared to dark conditions.

Within the prodrug design, we report the first visible-light-induced cleavage of a $C(sp^3)-C(sp^3)$ bond to release the electrophilic, *ortho-* and *para-*quinone moieties of the isomeric β - and α -lapachones, respectively. Investigations into the photorelease mechanisms support an intramolecular charge-transfer event upon excitation that facilitates bond cleavage via a proposed radical pathway.

We envision that cleavable C–C bonds can be further investigated to enable effective masking and release of other substrates that previously could not be employed in photocaged designs for various time-resolved applications. Since phototherapeutics applied in vivo (e.g., photodynamic therapy) use fiber optics to deliver light to the tumors, it is possible for the short 420 nm wavelength light required to

activate 1 to reach the tumor, and blue light is clinically used in PDT for some skin cancer therapies and other skin conditions;⁵⁷ however, poor light penetration within the tumor at ~1 mm in depth is expected.⁵⁸ We are currently investigating the use of redshifted photocages to improve tumor tissue penetration for future in vivo applications. As well, further investigations in alternative mechanisms of bond cleavage for other existing photoremovable protecting groups beyond DEACM may change traditional understandings. Broader insight of photocaged excited states and pathways would enable rapid expansion of current photocleavable protecting groups to be utilized for nontraditional substrates. Additionally, our strategy can facilitate appropriate design of new photocage classes that are of instrumental use to research fields that utilize light for precise activation of substrate function.

■ EXPERIMENTAL SECTION

Computational Details. DFT calculations were performed using the Gaussian16 package.⁵⁹ All geometry optimizations were performed at the B3LYP level of theory⁶⁰ without any constraints at 298 K and 1 atm using an ultrafine integration grid and Grimme's D3 dispersion⁶¹ with Becke-Johnson damping.⁶² The Berny algorithm⁶³ was used for geometry optimizations. The 6-31+g(d,p) Pople basis set^{64–66} was used for all atoms. All frequency calculations were performed at the same level of theory for all intermediates and transition states to confirm minima (no imaginary frequencies) or first-order saddle points (exactly one imaginary frequency). Transition states were confirmed by intrinsic reaction coordinate calculations.⁶⁷ TD-DFT calculations were performed at the same level of theory. Following geometry optimization, electronic energies of the optimized structures were recalculated at the M06-2x level of theory⁶⁸ with the addition of Grimme's D3 dispersion with the original damping function. 61 Dunning's augmented correlation consistent triple- ζ basis set aug-cc-pvtz⁶⁹ was used for all atoms. Solvent effects were assessed using the SMD model developed by Truhlar⁷⁰ using default parameters for water. We note that ground-state DFT and excitedstate TD-DFT calculations with implicit solvent models may be prone to errors for neutral and ionic pairs due to the fact that these methods do not account for specific solute—solvent interactions. Minnesota functionals were recently used to assess photocage cleavage. Solution phase-corrected zero-point energies, enthalpies, and Gibbs free energies were obtained by adding the respective gas-phase thermodynamic contributions to the single-point energies. The solution-phase Gibbs free energies were calculated using the following equations.

$$G_{\rm sol} = G_{\rm gas} + G_{\rm solv} \tag{1}$$

$$G_{\rm gas} = H_{\rm gas} - TS_{\rm gas} \tag{2}$$

$$H_{\rm gas} = E_{\rm SCF} + \rm ZPE \tag{3}$$

where $G_{\rm solv}$ represents the Gibbs free energy with solvation correction, $G_{\rm solv}$ from the gas-phase Gibbs free energy $G_{\rm gas}$. $H_{\rm gas}$ refers to the enthalpy of the species in the gas phase, T is the temperature, and $S_{\rm gas}$ is the entropy of the molecule in the gas phase. $E_{\rm SCF}$ refers to the self-consistent field electronic energy, and ZPE refers to the zero-point energy. Gibbs free energies are reported in kilocalorie per mole. The Gibbs free energies were converted to standard state by applying a correction of 1.89 kcal mol⁻¹ to all species [according to RT ln $(c/c_0)^{71}$ at 298.15 K]. Grimme's quasi-harmonic approximation was used with a frequency cutoff of 50 cm⁻¹, as recommended by Baik, 72 to correct for the effect of small-frequency vibrational modes. The images of the computed structures were created with CYLview (unimportant hydrogens omitted for clarity).

ASSOCIATED CONTENT

Supporting Information

The Supporting Information is available free of charge at https://pubs.acs.org/doi/10.1021/jacs.3c00398.

Synthetic details; ¹H, ¹³C NMR, and HRMS spectra; photophysical characterization experiments; NMR experiments; UV–vis and fluorescence spectroscopy; quantum yield measurements; EPR experiment; energies and cartesian coordinates; cell culture details; imaging experiments; and cell viability experiments (PDF)

Accession Codes

CCDC 2235658–2235659 contain the supplementary crystallographic data for this paper. These data can be obtained free of charge via www.ccdc.cam.ac.uk/data_request/cif, or by emailing data_request/cif, or by contacting The Cambridge Crystallographic Data Centre, 12 Union Road, Cambridge CB2 1EZ, UK; fax: +44 1223 336033.

AUTHOR INFORMATION

Corresponding Author

Andrew A. Beharry — Department of Chemical and Physical Sciences, University of Toronto Mississauga, Mississauga, Ontario L5L 1C6, Canada; Department of Chemistry, University of Toronto, Toronto, Ontario MSS 3H6, Canada; orcid.org/0000-0003-1505-2375; Email: andrew.beharry@utoronto.ca

Authors

Esther G. Kaye — Department of Chemical and Physical Sciences, University of Toronto Mississauga, Mississauga, Ontario L5L 1C6, Canada; Department of Chemistry, University of Toronto, Toronto, Ontario MSS 3H6, Canada; orcid.org/0000-0002-4357-0914

Bijan Mirabi – Department of Chemistry, Davenport Chemical Laboratories, University of Toronto, Toronto, Ontario MSS 3H6, Canada; © orcid.org/0000-0002-4852-3439

Ivonne R. Lopez-Miranda — Department of Chemical and Physical Sciences, University of Toronto Mississauga, Mississauga, Ontario LSL 1C6, Canada; Department of Chemistry, University of Toronto, Toronto, Ontario MSS 3H6, Canada

Komadhie C. Dissanayake — Department of Chemistry, Iowa State University, Ames, Iowa 50014, United States; orcid.org/0000-0003-3347-1004

Upasana Banerjee - Department of Chemistry, Iowa State University, Ames, Iowa 50014, United States; ⊙ orcid.org/ 0000-0002-5580-4511

Madelyn Austin – Department of Chemistry, Iowa State University, Ames, Iowa 50014, United States

Mark Lautens — Department of Chemistry, Davenport Chemical Laboratories, University of Toronto, Toronto, Ontario M5S 3H6, Canada; orcid.org/0000-0002-0179-2914

Arthur H. Winter — Department of Chemistry, Iowa State University, Ames, Iowa 50014, United States; ⊚ orcid.org/0000-0003-2421-5578

Complete contact information is available at: https://pubs.acs.org/10.1021/jacs.3c00398

Notes

The authors declare no competing financial interest.

ACKNOWLEDGMENTS

A.A.B. and M.L. acknowledge funding from the Natural Sciences and Engineering Research Council of Canada (NSERC) Discovery Grant. E.G.K. thanks the Province of Ontario (QEII-GSST), and B.M. thanks NSERC (CGS-D) for funding. I.R.L.-M. thanks support from the University of Toronto Excellence Award (UTEA). Computational studies were enabled in part through support provided by Compute Ontario (www.computeontario.ca) and Compute Canada (www.computercanada.ca). We thank Dr. Alan Lough (University of Toronto) for X-ray crystallographic analysis. Many thanks to Dr. Darcy Burns, Dr. Jack Sheng, and Dmitry Pichuigin (University of Toronto) for their assistance and support with NMR and EPR experiments. A.H.W. thanks NSF (CHE-2055335).

REFERENCES

(1) Atanasov, A. G.; Zotchev, S. B.; Dirsch, V. M.; Orhan, I. E.; Banach, M.; Rollinger, J. M.; Barreca, D.; Weckwerth, W.; Bauer, R.; Bayer, E. A.; Majeed, M.; Bishayee, A.; Bochkov, V.; Bonn, G. K.; Braidy, N.; Bucar, F.; Cifuentes, A.; D'Onofrio, G.; Bodkin, M.; Diederich, M.; Dinkova-Kostova, A. T.; Efferth, T.; El Bairi, K.; Arkells, N.; Fan, T. P.; Fiebich, B. L.; Freissmuth, M.; Georgiev, M. I.; Gibbons, S.; Godfrey, K. M.; Gruber, C. W.; Heer, J.; Huber, L. A.; Ibanez, E.; Kijjoa, A.; Kiss, A. K.; Lu, A.; Macias, F. A.; Miller, M. J. S.; Mocan, A.; Müller, R.; Nicoletti, F.; Perry, G.; Pittalà, V.; Rastrelli, L.; Ristow, M.; Russo, G. L.; Silva, A. S.; Schuster, D.; Sheridan, H.; Skalicka-Woźniak, K.; Skaltsounis, L.; Sobarzo-Sánchez, E.; Bredt, D. S.; Stuppner, H.; Sureda, A.; Tzvetkov, N. T.; Vacca, R. A.; Aggarwal, B. B.; Battino, M.; Giampieri, F.; Wink, M.; Wolfender, J. L.; Xiao, J.; Yeung, A. W. K.; Lizard, G.; Popp, M. A.; Heinrich, M.; Berindan-Neagoe, I.; Stadler, M.; Daglia, M.; Verpoorte, R.; Supuran, C. T. Natural Products in Drug Discovery: Advances and Opportunities. Nat. Rev. Drug Discovery 2021, 20, 200-216.

(2) Gómez Castellanos, J. R.; Prieto, J. M.; Heinrich, M. Red Lapacho (Tabebuia Impetiginosa) - A Global Ethnopharmacological Commodity? *J. Ethnopharmacol.* **2009**, *121*, 1–13.

- (3) Yang, Y.; Zhou, X.; Xu, M.; Piao, J.; Zhang, Y.; Lin, Z.; Chen, L. β -Lapachone Suppresses Tumour Progression by Inhibiting Epithelial-to-Mesenchymal Transition in NQO1-Positive Breast Cancers. *Sci. Rep.* **2017**, *7*, 2681.
- (4) Bey, E. A.; Reinicke, K. E.; Srougi, M. C.; Varnes, M.; Anderson, V. E.; Pink, J. J.; Li, L. S.; Patel, M.; Cao, L.; Moore, Z.; Rommel, A.; Boatman, M.; Lewis, C.; Euhus, D. M.; Bornmann, W. G.; Buchsbaum, D. J.; Spitz, D. R.; Gao, J.; Boothman, D. A. Catalase Abrogates β -Lapachone-Induced PARP1 Hyperactivation-Directed Programmed Necrosis in NQO1-Positive Breast Cancers. *Mol. Cancer Ther.* **2013**, *12*, 2110–2120.
- (5) Planchon, S. M.; Pink, J. J.; Tagliarino, C.; Bornmann, W. G.; Varnes, M. E.; Boothman, D. A. β -Lapachone-Induced Apoptosis in Human Prostate Cancer Cells: Involvement of NQO1/Xip3. *Exp. Cell Res.* **2001**, 267, 95–106.
- (6) Lee, J. H.; Cheong, J. H.; Park, Y. M.; Choi, Y. H. Down-Regulation of Cyclooxygenase-2 and Telomerase Activity by β -Lapachone in Human Prostate Carcinoma Cells. *Pharmacol. Res.* **2005**, *51*, 553–560.
- (7) Ough, M.; Lewis, A.; Bey, E. A.; Gao, J.; Ritchie, J. M.; Bornmann, W.; Boothman, D. A.; Oberley, L. W.; Cullen, J. J. Efficacy of β -Lapachone in Pancreatic Cancer Treatment: Exploiting the Novel, Therapeutic Target NQO1. *Cancer Biol. Ther.* **2005**, *4*, 102–109.
- (8) Silvers, M. A.; Deja, S.; Singh, N.; Egnatchik, R. A.; Sudderth, J.; Luo, X.; Beg, M. S.; Burgess, S. C.; DeBerardinis, R. J.; Boothman, D. A.; Merritt, M. E. The NQO1 bioactivatable drug, β -lapachone, alters the redox state of NQO1+ pancreatic cancer cells, causing perturbation in central carbon metabolism. *J. Biol. Chem.* **2017**, 292, 18203–18216.
- (9) Zhao, W.; Jiang, L.; Fang, T.; Fang, F.; Liu, Y.; Zhao, Y.; You, Y.; Zhou, H.; Su, X.; Wang, J.; Liu, S.; Chen, Y.; Wan, J.; Huang, X. β -Lapachone Selectively Kills Hepatocellular Carcinoma Cells by Targeting NQO1 to Induce Extensive DNA Damage and PARP1 Hyperactivation. *Front. Oncol.* **2021**, *11*, 747282.
- (10) Park, E. J.; Min, K. J.; Lee, T. J.; Yoo, Y. H.; Kim, Y. S.; Kwon, T. K. β -Lapachone Induces Programmed Necrosis through the RIP1-PARP-AIF-Dependent Pathway in Human Hepatocellular Carcinoma SK-Hep1 Cells. *Cell Death Dis.* **2014**, *5*, 12300.
- (11) Kee, J. Y.; Han, Y. H.; Kim, D. S.; Mun, J. G.; Park, S. H.; So, H. S.; Park, S. J.; Park, R.; Um, J. Y.; Hong, S. H. β -Lapachone Suppresses the Lung Metastasis of Melanoma via the MAPK Signaling Pathway. *PLoS One* **2017**, *12*, 01769377.
- (12) Dong, G. Z.; Oh, E. T.; Lee, H.; Park, M. T.; Song, C. W.; Park, H. J. β-Lapachone Suppresses Radiation-Induced Activation of Nuclear Factor-KB. *Exp. Mol. Med.* **2010**, *42*, 327–334.
- (13) Bey, E. A.; Bentle, M. S.; Reinicke, K. E.; Dong, Y.; Yang, C. R.; Girard, L.; Minna, J. D.; Bornmann, W. G.; Gao, J.; Boothman, D. A. An NQO1- and PARP-1-Mediated Cell Death Pathway Induced in Non-Small-Cell Lung Cancer Cells by β -Lapachone. *Proc. Natl. Acad. Sci. U.S.A.* **2007**, *104*, 11832—11837.
- (14) Planchon, S. M.; Wuerzberger, S.; Boothman, D. A.; Church, D. R.; Wilding, G.; Frydman, B.; Witiak, D. T.; Hutson, P. β -Lapachone-Mediated Apoptosis in Human Promyelocytic Leukemia (HL-60) and Human Prostate Cancer Cells: A P53-Independent Response. *Cancer Res.* **1995**, *55*, 3706–3711.
- (15) Bey, E. A.; Wuerzberger-Davis, S. M.; Pink, J. J.; Yang, C. R.; Araki, S.; Reinicke, K. E.; Bentle, M. S.; Dong, Y.; Cataldo, E.; Criswell, T. L.; Wagner, M. W.; Li, L.; Gao, J.; Boothman, D. A. Mornings with Art, Lessons Learned: Feedback Regulation, Restriction Threshold Biology, and Redundancy Govern Molecular Stress Responses. J. Cell. Physiol. 2006, 209, 604–610.
- (16) Pink, J. J.; Planchon, S. M.; Tagliarino, C.; Varnes, M. E.; Siegel, D.; Boothman, D. A. NAD(P)H:Quinone Oxidoreductase Activity Is the Principal Determinant of β -Lapachone Cytotoxicity. *J. Biol. Chem.* **2000**, 275, 5416–5424.
- (17) Vanni, A.; Fiore, M.; De Salvia, R.; Cundari, E.; Ricordy, R.; Ceccarelli, R.; Degrassi, F. DNA Damage and Cytotoxicity Induced by

- β -Lapachone: Relation to Poly(ADP-Ribose) Polymerase Inhibition. *Mutat. Res.* **1998**, *401*, 55–63.
- (18) Tagliarino, C.; Pink, J. J.; Dubyak, G. R.; Nieminen, A. L.; Boothman, D. A. Calcium Is a Key Signaling Molecule in β -Lapachone-Mediated Cell Death. *J. Biol. Chem.* **2001**, 276, 19150–19159.
- (19) Gong, Q.; Hu, J.; Wang, P.; Li, X.; Zhang, X. A Comprehensive Review on β -Lapachone: Mechanisms, Structural Modifications, and Therapeutic Potentials. *Eur. J. Med. Chem.* **2021**, 210, 112962.
- (20) Ross, D.; Siegel, D. Functions of NQO1 in Cellular Protection and CoQ10 Metabolism and Its Potential Role as a Redox Sensitive Molecular Switch. *Front. Physiol.* **2017**, *8*, 595.
- (21) Gerber, D. E.; Beg, M. S.; Fattah, F.; Frankel, A. E.; Fatunde, O.; Arriaga, Y.; Dowell, J. E.; Bisen, A.; Leff, R. D.; Meek, C. C.; Putnam, W. C.; Kallem, R. R.; Subramaniyan, I.; Dong, Y.; Bolluyt, J.; Sarode, V.; Luo, X.; Xie, Y.; Schwartz, B.; et al. Phase 1 Study of ARQ 761, a β -Lapachone Analogue That Promotes NQO1-Mediated Programmed Cancer Cell Necrosis. *Br. J. Cancer* **2018**, *119*, 928–936.
- (22) Dunsmore, L.; Navo, C. D.; Becher, J.; de Montes, E. G.; Guerreiro, A.; Hoyt, E.; Brown, L.; Zelenay, V.; Mikutis, S.; Cooper, J.; Barbieri, I.; Lawrinowitz, S.; Siouve, E.; Martin, E.; Ruivo, P. R.; Rodrigues, T.; da Cruz, F. P.; Werz, O.; Vassiliou, G.; Ravn, P.; Jiménez-Osés, G.; Bernardes, G. J. L. Controlled Masking and Targeted Release of Redox-Cycling Ortho-Quinones via a C-C Bond-Cleaving 1,6-Elimination. *Nat. Chem.* 2022, 14, 754–765.
- (23) Gong, Q.; Li, X.; Li, T.; Wu, X.; Hu, J.; Yang, F.; Zhang, X. A Carbon-Carbon Bond Cleavage-Based Prodrug Activation Strategy Applied to β -Lapachone for Cancer-Specfic Targeting. *Angew. Chem., Int. Ed.* **2022**, *61*, No. e202210001.
- (24) Pellois, J. P.; Hahn, M. E.; Muir, T. W. Simultaneous Triggering of Protein Activity and Fluorescence. *J. Am. Chem. Soc.* **2004**, *126*, 7170–7171.
- (25) Ottl, J.; Gabriel, D.; Marriott, G. Preparation and Photo-activation of Caged Fluorophores and Caged Proteins Using a New Class of Heterobifunctional, Photocleavable Cross-Linking Reagents. *Bioconjugate Chem.* **1998**, *9*, 143–151.
- (26) Gautier, A.; Nguyen, D. P.; Lusic, H.; An, W.; Deiters, A.; Chin, J. W. Genetically Encoded Photocontrol of Protein Localization in Mammalian Cells. *J. Am. Chem. Soc.* **2010**, *132*, 4086–4088.
- (27) Aonbangkhen, C.; Zhang, H.; Wu, D. Z.; Lampson, M. A.; Chenoweth, D. M. Reversible Control of Protein Localization in Living Cells Using a Photocaged-Photocleavable Chemical Dimerizer. *J. Am. Chem. Soc.* **2018**, *140*, 11926–11930.
- (28) Gaur, P.; Kucherak, O. A.; Ermakova, Y. G.; Shvadchak, V. V.; Yushchenko, D. A. Nitrobenzyl-Based Fluorescent Photocages for Spatial and Temporal Control of Signalling Lipids in Cells. *Chem. Commun.* **2019**, *55*, 12288–12291.
- (29) Skwarczynski, M.; Noguchi, M.; Hirota, S.; Sohma, Y.; Kimura, T.; Hayashi, Y.; Kiso, Y. Development of First Photoresponsive Prodrug of Paclitaxel. *Bioorg. Med. Chem. Lett.* **2006**, *16*, 4492–4496.
- (30) Contreras-García, E.; Lozano, C.; García-Iriepa, C.; Marazzi, M.; Winter, A. H.; Torres, C.; Sampedro, D. Controlling Antimicrobial Activity of Quinolones Using Visible/NIR Light-Activated BODIPY Photocages. *Pharmaceutics* **2022**, *14*, 1070.
- (31) Yamaguchi, S.; Chen, Y.; Nakajima, S.; Furuta, T.; Nagamune, T. Light-Activated Gene Expression from Site-Specific Caged DNA with a Biotinylated Photolabile Protection Group. *Chem. Commun.* **2010**, *46*, 2244–2246.
- (32) Park, C. H.; Givens, R. S. New Photoactivated Protecting Groups. 6. p-Hydroxyphenacyl: A Phototrigger for Chemical and Biochemical Probes. *J. Am. Chem. Soc.* **1997**, *119*, 2453–2463.
- (33) Sheehan, J. C.; Wilson, R. M.; Oxford, A. W. Photolysis of methoxy-substituted benzoin esters. Photosensitive protecting group for carboxylic acids. *J. Am. Chem. Soc.* **1971**, *93*, 7222–7228.
- (34) Corrie, J. E. T.; Barth, A.; Munasinghe, V. R. N.; Trentham, D. R.; Hutter, M. C. Photolytic Cleavage of 1-(2-Nitrophenyl)Ethyl Ethers Involves Two Parallel Pathways and Product Release Is Rate-Limited by Decomposition of a Common Hemiacetal Intermediate. *J. Am. Chem. Soc.* 2003, 125, 8546–8554.

- (35) Givens, R. S.; Matuszewski, B. Photochemistry of Phosphate Esters: An Efficient Method for the Generation of Electrophiles. J. Am. Chem. Soc. 1984, 106, 6860-6861.
- (36) Fedoryak, O. D.; Dore, T. M. Brominated Hydroxyguinoline as a Photolabile Protecting Group with Sensitivity to Multiphoton Excitation. Org. Lett. 2002, 4, 3419-3422.
- (37) Peterson, J. A.; Wijesooriya, C.; Gehrmann, E. J.; Mahoney, K. M.; Goswami, P. P.; Albright, T. R.; Syed, A.; Dutton, A. S.; Smith, E. A.; Winter, A. H. Family of BODIPY Photocages Cleaved by Single Photons of Visible/Near-Infrared Light. J. Am. Chem. Soc. 2018, 140,
- (38) Rubinstein, N.; Liu, P.; Miller, E. W.; Weinstain, R. Meso-Methylhydroxy BODIPY: A Scaffold for Photo-Labile Protecting Groups. Chem. Commun. 2015, 51, 6369-6372.
- (39) Klán, P.; Šolomek, T.; Bochet, C. G.; Blanc, A.; Givens, R.; Rubina, M.; Popik, V.; Kostikov, A.; Wirz, J. Photoremovable Protecting Groups in Chemistry and Biology: Reaction Mechanisms and Efficacy. Chem. Rev. 2013, 113, 119-191.
- (40) Sitkowska, K.; Feringa, B. L.; Szymański, W. Green-Light-Sensitive BODIPY Photoprotecting Groups for Amines. J. Org. Chem. 2018, 83, 1819-1827.
- (41) Huynh, T. H. V.; Abrahamsen, B.; Madsen, K. K.; Gonzalez-Franquesa, A.; Jensen, A. A.; Bunch, L. Design, Synthesis and Pharmacological Characterization of Coumarin-Based Fluorescent Analogs of Excitatory Amino Acid Transporter Subtype 1 Selective Inhibitors, UCPH-101 and UCPH-102. Bioorg. Med. Chem. 2012, 20, 6831-6839.
- (42) Wong, P. T.; Roberts, E. W.; Tang, S.; Mukherjee, J.; Cannon, J.; Nip, A. J.; Corbin, K.; Krummel, M. F.; Choi, S. K. Control of an Unusual Photo-Claisen Rearrangement in Coumarin Caged Tamoxifen through an Extended Spacer. ACS Chem. Biol. 2017, 12, 1001-
- (43) Jones, G.; Jackson, W. R.; Choi, C. Y.; Bergmark, W. R. Solvent Effects on Emission Yield and Lifetime for Coumarin Laser Dyes. Requirements for a Rotatory Decay Mechanism. J. Phys. Chem. 1985, 89, 294-300.
- (44) Schade, B.; Hagen, V.; Schmidt, R.; Herbrich, R.; Krause, E.; Eckardt, T.; Bendig, J. Deactivation Behavior and Excited-State Properties of (Coumarin-4- Yl)Methyl Derivatives. 1. Photocleavage of (7-Methoxycoumarin-4-Yl)Methyl- Caged Acids with Fluorescence Enhancement. J. Org. Chem. 1999, 64, 9109-9117.
- (45) The inner filter effect created by the coumarin by-products' absorption is likely responsible for the lack of full conversion observed at the administered light dosages.
- (46) Schoenleber, R. O.; Giese, B. Photochemical Release of Amines by C,N-Bond Cleavage. Synlett 2003, 2003, 501-504.
- (47) Schulte, A. M.; Alachouzos, G.; Szymański, W.; Feringa, B. L. Strategy for Engineering High Photolysis Efficiency of Photocleavable Protecting Groups through Cation Stabilization. J. Am. Chem. Soc. 2022, 144, 12421-12430.
- (48) Yip, R. W.; Wen, Y. X. Photophysics of 7-Diethylamino-4-Methylcoumarin: Picosecond Time-Resolved Absorption and Amplified Emission Study. J. Photochem. Photobiol. 1990, 54, 263-270.
- (49) Villamil, S. F.; Stoppani, A. O. M.; Dubin, M. Redox Cycling of β-Lapachone and Structural Analogues in Microsomal and Cytosol Liver Preparations. Methods Enzymol. 2004, 378, 67-87.
- (50) A proposed mechanism for the regioselective outcome of products based on the nature of the electrophile is noted in the Supporting Information (Scheme S2).
- (51) Ferreira, V. F.; de Carvalho, A. S.; Ferreira, P. G.; Lima, C. G.; de C da Silva, F.; da Silva, F. d. C. Quinone-Based Drugs: An Important Class of Molecules in Medicinal Chemistry. Med. Chem. 2021, 17, 1073-1085.
- (52) Bolzán, A. D.; Bianchi, M. S. Genotoxicity of Streptonigrin: A Review. Mutat. Res. 2001, 488, 25-37.
- (53) Miao, X.; Song, P.; Savage, R. E.; Zhong, C.; Yang, R.; Kizer, D.; Wu, H.; Volckova, E.; Ashwell, M. A.; Supko, J. G.; He, X.; Chan, T. C. K. Identification of the in Vitro Metabolites of 3, 4-Dihydro-2, 2- Dimethyl-2 H -Naphthol [1, 2-b] Pyran-5, 6-Dione (ARQ 501;

- β-Lapachone) in Whole Blood. Drug Metab. Dispos. 2008, 36, 641-
- (54) Kim, I.; Kim, H.; Ro, J.; Jo, K.; Karki, S.; Khadka, P.; Yun, G.; Lee, J. Preclinical Pharmacokinetic Evaluation of β -Lapachone : Characteristics of Oral Bioavailability and First-Pass Metabolism in Rats. Biomol. Ther. 2015, 23, 296-300.
- (55) Cao, L.; Li, L. S.; Spruell, C.; Xiao, L.; Chakrabarti, G.; Bey, E. A.; Reinicke, K. E.; Srougi, M. C.; Moore, Z.; Dong, Y.; Vo, P.; Kabbani, W.; Yang, C. R.; Wang, X.; Fattah, F.; Morales, J. C.; Motea, E. A.; Bornmann, W. G.; Yordy, J. S.; Boothman, D. A. Tumor-Selective, Futile Redox Cycle-Induced Bystander Effects Elicited by NQO1 Bioactivatable Radiosensitizing Drugs in Triple-Negative Breast Cancers. Antioxid. Redox Signaling 2014, 21, 237-250.
- (56) Huang, X.; Dong, Y.; Bey, E. A.; Kilgore, J. A.; Bair, J. S.; Li, L. S.; Patel, M.; Parkinson, E. I.; Wang, Y.; Williams, N. S.; Gao, J.; Hergenrother, P. J.; Boothman, D. A. An NQO1 Substrate with Potent Antitumor Activity That Selectively Kills by PARP1-Induced Programmed Necrosis. Cancer Res. 2012, 72, 3038-3047.
- (57) Touma, D.; Yaar, M.; Whitehead, S.; Konnikov, N.; Gilchrest, B. A. A Trial of Short Incubation, Broad-Area Photodynamic Therapy for Facial Actinic Keratoses and Diffuse Photodamage. Arch. Dermatol. 2004, 140, 33.
- (58) Douplik, A.; Saiko, G.; Schelkanova, I.; Tuchin, V. V. 3 The Response of Tissue to Laser Light. In Lasers for Medical Applications; Woodhead Publishing, 2013; pp 47-109.
- (59) Frisch, M. J.; Trucks, G. W.; Schlegel, H. B.; Scuseria, G. E.; Robb, M. A.; Cheeseman, J. R.; Scalmani, G.; Barone, V.; Petersson, G. A.; Nakatsuji, H.; Li, X.; Caricato, M.; Marenich, A. V.; Bloino, J.; Janesko, B. G.; Gomperts, R.; Mennucci, B.; Hratchian, H. P.; Ortiz, J. V.; Izmaylov, A. F.; Sonnenberg, J. L.; Williams-Young, D.; Ding, F.; Lipparini, F.; Egidi, F.; Goings, J.; Peng, B.; Petrone, A.; Henderson, T.; Ranasinghe, D.; Zakrzewski, V. G.; Gao, J.; Rega, N.; Zheng, G.; Liang, W.; Hada, M.; Ehara, M.; Toyota, K.; Fukuda, R.; Hasegawa, J.; Ishida, M.; Nakajima, T.; Honda, Y.; Kitao, O.; Nakai, H.; Vreven, T.; Throssell, K.; Montgomery, J. A., Jr.; Peralta, J. E.; Ogliaro, F.; Bearpark, M. J.; Heyd, J. J.; Brothers, E. N.; Kudin, K. N.; Staroverov, V. N.; Keith, T. A.; Kobayashi, R.; Normand, J.; Raghavachari, K.; Rendell, A. P.; Burant, J. C.; Iyengar, S. S.; Tomasi, J.; Cossi, M.; Millam, J. M.; Klene, M.; Adamo, C.; Cammi, R.; Ochterski, J. W.; Martin, R. L.; Morokuma, K.; Farkas, O.; Foresman, J. B.; Fox, D. J. Gaussian 16 package; Guassian, Inc.: Wallingford CT, 2016.
- (60) Becke, A. D. Density-Functional Thermochemistry. III. The Role of Exact Exchange. J. Chem. Phys. 1993, 98, 5648-5652.
- (61) Grimme, S.; Antony, J.; Ehrlich, S.; Krieg, H. A consistent and accurate ab initio parametrization of density functional dispersion correction (DFT-D) for the 94 elements H-Pu. J. Chem. Phys. 2010, 132, 154104.
- (62) Grimme, S.; Ehrlich, S.; Goerigk, L. Effect of the Damping Function in Dispersion Corrected Density Functional Theory. J. Comput. Chem. 2011, 32, 1456-1465.
- (63) Li, X.; Frisch, M. J. Energy-Represented Direct Inversion in the Iterative Subspace within a Hybrid Geometry Optimization Method. J. Chem. Theory Comput. 2006, 2, 835-839.
- (64) Petersson, G. A.; Bennett, A.; Tensfeldt, T. G.; Al-Laham, M. A.; Shirley, W. A.; Mantzaris, J. A complete basis set model chemistry. I. The total energies of closed-shell atoms and hydrides of the firstrow elements. J. Chem. Phys. 1988, 89, 2193-2218.
- (65) Petersson, G. A.; Al-Laham, M. A. A Complete Basis Set Model Chemistry. II. Open-Shell Systems and the Total Energies of the First-Row Atoms. J. Chem. Phys. 1991, 94, 6081-6090.
- (66) Clark, T.; Chandrasekhar, J.; Spitznagel, G. W.; Schleyer, P. v. R. Efficient diffuse function-augmented basis sets for anion calculations. III. The 3-21+G basis set for first-row elements, Li-F. J. Comput. Chem. 1983, 4, 294-301.
- (67) Fukui, K. The Path of Chemical Reactions The IRC Approach. Acc. Chem. Res. 1981, 14, 363-368.
- (68) Zhao, Y.; Truhlar, D. G. The M06 suite of density functionals for main group thermochemistry, thermochemical kinetics, noncovalent interactions, excited states, and transition elements: two new

- functionals and systematic testing of four M06-class functionals and 12 other functionals. *Theor. Chem. Acc.* **2008**, *120*, 215–241.
- (69) Kendall, R. A.; Dunning, T. H., Jr.; Harrison, R. J. Electron Affinities of the First-Row Atoms Revisited. Systematic Basis Sets and Wave Functions. *J. Chem. Phys.* **1992**, *96*, 6796–6806.
- (70) Marenich, A. V.; Cramer, C. J.; Truhlar, D. G. Universal Solvation Model Based on Solute Electron Density and on a Continuum Model of the Solvent Defined by the Bulk Dielectric Constant and Atomic Surface Tensions. *J. Phys. Chem. B* **2009**, *113*, 6378–6396.
- (71) Hopmann, K. H. How Accurate Is DFT for Iridium-Mediated Chemistry? *Organometallics* **2016**, *35*, 3795–3807.
- (72) Ryu, H.; Park, J.; Kim, H. K.; Park, J. Y.; Kim, S. T.; Baik, M. H. Pitfalls in Computational Modeling of Chemical Reactions and How to Avoid Them. *Organometallics* **2018**, *37*, 3228–3239.
- (73) These calculations were carried out with the Python Script GoodVibes. Funes-Ardoiz, I. and Paton R. S. GoodVibes.py. https://doi.org/10.5281/zeonodo.124756.
- (74) Legault, C. Y. CYLview20, Université de Sherbrooke, Sherbrooke, Quebec, Canada, 2009, http://www.cylview.org.